Viscoelastic behavior of a mass-rubber band oscillator

A. Filipponi, L. Di Michele, and C. Ferrante

Citation: Am. J. Phys. **78**, 437 (2010); doi: 10.1119/1.3276052
View online: http://dx.doi.org/10.1119/1.3276052
View Table of Contents: http://ajp.aapt.org/resource/1/AJPIAS/v78/i4
Published by the American Association of Physics Teachers

Viscoelastic behavior of a mass-rubber band oscillator

A. Filipponi, L. Di Michele, and C. Ferrante
Dipartimento di Fisica, Università degli Studi dell'Aquila, 67100 Coppito (AQ), Italy

(Received 4 May 2009; accepted 30 November 2009)

The behavior of a one-dimensional mass-rubber band oscillator is investigated experimentally. The data show clear evidence for viscoelastic behavior and can be interpreted in terms of a simple oscillator model consisting of a mass connected to a four parameter viscoelastic element. The model displays the observed crossover in the dynamic response. The success and limitations of the model and the pedagogical relevance of the experiment are discussed. © *2010 American Association of Physics Teachers.*

[DOI: 10.1119/1.3276052]

I. INTRODUCTION

One-dimensional mechanical oscillators are useful for introducing and applying basic physical concepts and illustrating the use of differential equations. Popular topics include harmonic systems and nonlinear oscillators such as the pendulum.[1–4] Damped oscillator models are useful for illustrating the role of friction in simple mechanical systems.[5–10]

A very simple oscillator with much pedagogical value can be built by connecting a mass to a rubber band. If we consider only the longitudinal degree of freedom involving rubber extension, such an oscillator is characterized by greater damping than an equivalent oscillator with a harmonic spring. This damping originates from the rubber band, and its modeling is a challenge for undergraduate students. Is a simple linear differential equation with viscous damping able to describe the motion? This investigation requires both experiments and modeling and comparison with the data. An investigation of the behavior of rubber in undergraduate courses is important because it provides a link to real world objects and a chance to establish the validity and limitations of simple models for a familiar material.

The physical properties of rubber are well known[11,12] and understood in terms of a network of cross-linked polymers. For our purposes the origin of the mechanical behavior of rubber is mainly due to the long relaxation times associated with the internal degrees of freedom of the polymeric structure currently understood within the theory of viscoelasticity.[13–15] Although viscoelasticity is usually beyond the scope of introductory physics courses, certain aspects can still be introduced, at least at a phenomenological level, and thus complement introductory textbooks and provide an interesting subject for further study.

In this paper we describe an experiment to acquire accurate kinematical data on a mass-rubber band oscillator. The experimental details are reported in Sec. II. In Sec. III we develop a model for a mechanical viscoelastic oscillator consisting of a mass attached to a linear viscoelastic solid element, and in Sec. IV we compare and discuss the data with the predictions of the model.

II. EXPERIMENTAL DETAILS

Viscoelastic material testing[14,15] is performed using a stress-strain apparatus where a material sample is subject to a known (periodic) strain, while the apparatus measures and records strain and stress data. This information, collected as a function of frequency, is able to characterize a viscoelastic material. Such a strategy is not suitable for a student laboratory where we often need many copies of the apparatus. Also the observation of free oscillations with a mass, which provides the required inertial contribution in the absence of a forcing term, facilitates establishing a simpler connection with common oscillating systems treated in basic mechanics courses. A few examples of viscoelastic testing using free oscillations are discussed in Refs. 14 and 15.

We have constructed a one-dimensional oscillator on a low friction horizontal rail, as illustrated in Fig. 1. A cart is connected to two identical rubber bands each with rest length $\ell_0=8.2$ cm. The rubber bands are fixed at the two sides on sliding brackets that allow us to adjust their extension. They were stretched to an equilibrium length $\ell \approx 2\ell_0$, corresponding to moderate stretching and roughly linear elastic response. The cart was made of an aluminum base rolling on three stainless steel spheres (diameter $2r=12$ mm and mass $m_s=18$ g) placed on parallel grooves between the rail and cart to achieve low friction. A similar system can be built using an air track. This system constitutes an effective one-dimensional oscillator whose position is given by the horizontal coordinate x. At rest the system remains in an equilibrium position $x=x_0$ with the cart in the middle. If the cart is displaced along the horizontal coordinate, the rubber bands act with a restoring force roughly proportional to the displacement from x_0. Investigating the actual nature of this force is the goal of the experiment. For this purpose the system can be displaced from the equilibrium position x_0 and observed during its free motion. The behavior of rubber can be compared to an equivalent oscillator obtained by replacing the rubber bands with harmonic springs.

This system can be described by a one-dimensional oscillator with a total mass m and a restoring force $F \approx -k(x-x_0)$ or possibly a more complex function. The period of the oscillations is roughly $T=2\pi\sqrt{m/k}$ and can be easily varied by nearly an order of magnitude by changing m. The effective mass m includes the mass of the cart and small inertial contributions from the three spheres and is equal to $3m_s\left(\frac{1}{4}+\frac{1}{10}(r/\rho)^2\right)$, where ρ is the contact radius. The mass of the rubber bands is negligible.

To acquire accurate kinematical information, we used an optical encoder made of a scale with equally spaced dark and transparent regions at $\approx$1 mm intervals rigidly fixed to the cart and parallel to the x coordinate. The passage of the dark/transparent edges was detected by a photogate fixed to the rail and connected to a digital interface on a personal computer, which allows for accurate timing of the events with μs resolution. This encoder is capable of acquiring position-time data for the motion of the cart with 10 μm (mostly limited

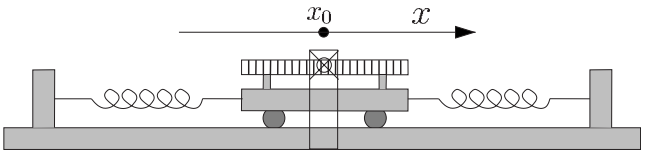

Fig. 1. Experimental configuration of a one-dimensional mass-rubber band oscillator. The rubber band extension at equilibrium can be adjusted by the fixed points on the movable side brackets. The optical encoder to determine $x(t)$ is made of a scale rigidly fixed to the cart and a photogate fixed to the rail system.

by the scale quality) and 10 μs accuracy sampled every mm. More details are given in the Appendix. These data can be used to calculate several kinematical quantities including average speed and acceleration and to estimate their instantaneous values.

Examples of data collected for different masses are shown in Fig. 2. The damping is dominated by the viscous behavior of the rubber bands, but a small dry friction contribution from the rolling cart is also present. The latter contribution was isolated by performing a similar experiment with harmonic springs and resulted in a dynamic dry friction coefficient μ_d=0.0002. The combination of viscous and dry friction[8] yields exponentially damped half-oscillations centered around alternatively displaced equilibrium positions according to the sign of the velocity. The dry friction term results in a constant force, which shifts the apparent equilibrium position, and its effect is evident only when the velocity changes sign, while the viscous friction acts with an exponential amplitude damping during the motion. The oscillation data were then fitted to the empirical function

$$x(t) = [Ae^{-\gamma t} - 2D(j+1)]\cos(\omega t + \phi) + D(-1)^j + x_0, \quad (1)$$

where j is the half-oscillation counter calculated as the integer part of $(\omega t+\phi)/\pi$ and $D=mg\mu_d/k \simeq g\mu_d/\omega^2$ is the dry friction equilibrium position shift. In the presence of dry friction, the mass reaches a rest state that does not necessarily coincide with the equilibrium position of the oscillator but is undetermined within the interval $(-D,D)$ (assuming identical static and dynamic friction coefficients) due to the fact that when the velocity is zero, the motion proceeds only if the restoring force is greater than the maximum possible static friction force modulus $F_s=mg\mu_s$. These details are not probed by the acquisition system because there is no sufficient number of data points when the amplitude of the oscillations is small. The dry friction correction is small and affects the fitted value of the γ parameter by only a few percent.

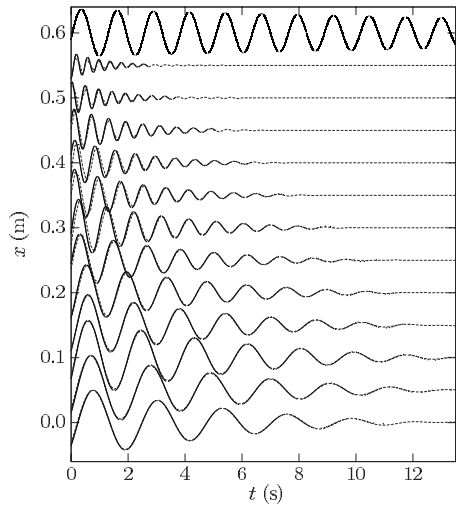

Fig. 2. Position versus time data for the mass-rubber band oscillator with different masses m according to Table I. The equilibrium positions are shifted by 0.05 m for clarity. The upper curve refers to a mass spring oscillator and shows the small effect of the rolling friction. The dashed curves are best fits to Eq. (1).

Although the overall agreement between the experimental data and the empirical form (1) is satisfactory, careful inspection reveals a slight phase mismatch as the damping of the oscillations proceeds. This mismatch cannot be explained by a linear oscillator model, which predicts a constant angular frequency ω and is an indication of small nonlinear effects in the elastic response leading to a slight increase of the angular frequency (by a few percent) as the system goes from larger to smaller amplitude motion. For this reason, although the amplitude parameters were fitted over the entire time range, the value of ω was fitted only in the second half of the temporal range corresponding to lower amplitude oscillations. Due to the accurate timing measurements, the period of a single oscillation can be determined to better than 1 part in 10^4. As a consequence the uncertainty in ω is limited only by the arbitrariness of the choice of the fitting range. Our procedure gave estimates of ω within 0.1%. The uncertainty in γ is limited by the model assumptions and is estimated to be about 2%–3%.

The results for the fitted parameters as a function of the oscillator mass m are reported in Table I. The dependence of the fitted parameters ω and γ as a function of the mass shown in Fig. 3 reveals interesting effects. A damped har-

Table I. Results for the empirical oscillation parameters ω and γ. The uncertainties are dominated by the limitations of the model and are discussed in the text.

m (kg)	ω (s^{-1})	γ (s^{-1})	m (kg)	ω (s^{-1})	γ (s^{-1})
0.18218	16.01	0.84	1.52184	5.385	0.22
0.25223	13.58	0.69	2.16682	4.488	0.18
0.41153	10.58	0.47	2.81096	3.922	0.16
0.55087	9.110	0.41	3.77560	3.366	0.14
0.71153	7.981	0.35	4.74338	2.990	0.13
1.03342	6.584	0.28	5.54318	2.764	0.14

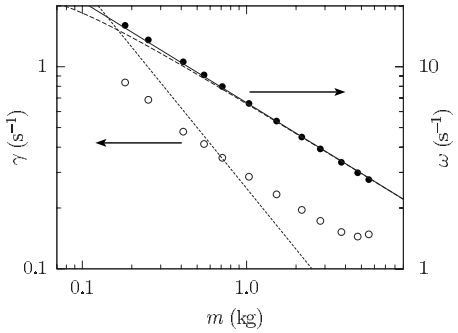

Fig. 3. Log-log plot of the angular frequency ω (●) and damping parameter γ (○) of the rubber band damped oscillator as a function of the mass m. Theoretical curves $\omega(m)$ for harmonic oscillators are also given: Solid line k=44 N/m no damping, dashed curve damped version with β=2 Ns/m. The dotted line is the damping parameter γ for a harmonic oscillator with β=0.5 Ns/m.

monic oscillator model of mass m, elastic constant k, and viscous friction $\vec{F}_f=-\beta\vec{v}$ is described by the differential equation

$$m\ddot{x}+\beta\dot{x}+kx=0. \tag{2}$$

For subcritical damping the oscillating solution is given by Eq. (1) with $x_0=0$, $D=0$, and

$$\gamma=\frac{\beta}{2m}<\omega_0=\sqrt{\frac{k}{m}}, \tag{3}$$

$$\omega=\sqrt{\omega_0^2-\gamma^2}, \quad m\omega^2=k-\frac{\beta^2}{4m}. \tag{4}$$

The experimental results are not in agreement with the prediction of this model. The γ parameter displays a much less pronounced mass dependence, indicating that the damping mechanism differs considerably from a simple viscous friction term. The data for ω deviate from the expected $\omega\propto m^{-1/2}$ behavior. In particular, this deviation (small on the scale of Fig. 3 but actually very important) indicates that for small masses and corresponding larger ω, the average angular frequency is larger than what is predicted for an harmonic oscillator with constant k. The deviation from the $\omega\approx\sqrt{k/m}$ behavior is opposite to the behavior predicted for a damped harmonic oscillator with constant β and k for which the effective angular frequency ω is less than ω_0 particularly for small masses.

III. THE VISCOELASTIC MODEL

To explain the observed mass dependence of the parameters, we require a more accurate model for the elastic response of the rubber band. In particular, in the framework of a linear model, the increased values of ω for small m can be explained only by introducing a dependence of the effective force constant k on the frequency. For small masses, and correspondingly smaller oscillation periods, the restoring force of the rubber band apparently acts with a larger effective force constant. This phenomenon can be understood in terms of viscoelastic behavior[13–15] and suggests the inclusion of internal viscoelastic degrees of freedom with appropriate relaxation times. Simple linear viscoelastic models can be represented using appropriate combinations of springs and

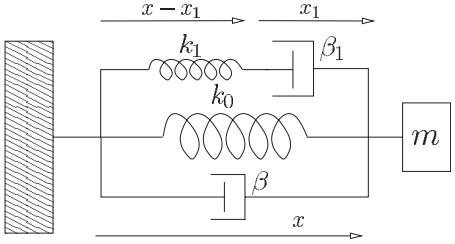

Fig. 4. A viscoelastic oscillator model with a mass m attached to a four parameter viscoelastic element. The internal coordinates of the dashpot x_1 and the spring on the viscoelastic element, with extension $x-x_1$, include the constraint of the common oscillator position x.

dashpots (viscous dampers). The model that we considered (see Fig. 4) is based on a viscous harmonic oscillator model (with parameters k_0 and β) to which a Maxwell element (that is, a secondary spring of elastic constant k_1 in series with a viscous damper with constant β_1) is added in parallel (the forces are additive). In the $\beta\to 0$ limit this model reduces to a standard linear solid model consisting of a spring in parallel to a Maxwell element.

The consideration of the more general model of Fig. 4 introduces only small algebraic complications to the solution. This model is intended to represent the linearized behavior of rubber in the neighborhood of the equilibrium position of the system with symmetrically stretched identical rubber bands. The parameters are twice those associated with a single rubber band. The viscoelastic element involves an internal degree of freedom x_1 characterized by a single relaxation time constant $\tau=\beta_1/k_1$. The behavior of such a viscoelastic system can be demonstrated by using a mechanical model. By displacing the end of the system at low frequency $\nu\ll 1/\tau$, the internal degree of freedom has time to follow the displacement of the end of the viscoelastic element. As a result the system behaves like a spring with elastic constant k_0. This behavior corresponds to what is expected during static measurements. At high frequency $\nu\gg 1/\tau$, the internal degree of freedom does not have time to relax, and the secondary spring has to follow the displacement of the end of the viscoelastic element. As a result the system behaves like a spring with elastic constant k_0+k_1. If such an element is connected to a mass m, the crossover between the two behaviors is determined by the value of the mass m. For $m\approx 0$ the system oscillates at high frequency, and the response is (k_0+k_1); for $m\to\infty$ the system oscillates at low frequency and the elastic response is k_0.

In the framework of viscoelastic theory,[13–15] such a model, with a single relaxation time, is very simplified. Nevertheless, it provides a first step toward a correct description of the system, and we will show that it is able to describe the experimental results. The usual treatment in the framework of the viscoelastic literature is based on rheological quantities and memory functions. One-dimensional viscoelastic oscillator models have been treated[16,17] using integrodifferential equations and Laplace transform methods leading to a detailed discussion of the nature of the solutions.[17] In this section we illustrate a solution based on mechanical quantities and linear differential equations, which is more suitable for undergraduates.

The equation of motion for the basic viscoelastic solid model can be written in the form of a system of coupled differential equations for x and x_1, one for the Maxwell ele-

ment, where the viscous and elastic forces are equal, and one for the entire system (the resulting force on the mass is the sum of the three forces in parallel),

$$\beta_1 \dot{x}_1 = k_1(x - x_1), \tag{5}$$

$$m\ddot{x} = -k_0 x - \beta_1 \dot{x}_1 - \beta \dot{x}. \tag{6}$$

The equilibrium coordinate is set to $x_0=0$ for simplicity. Equation (5) can be solved by considering $x(t)$ as an external forcing term, the solution is

$$x_1(t) = C_0 e^{-k_1 t/\beta_1} + \frac{k_1}{\beta_1}\int_{-\infty}^{t} e^{-k_1(t-t')/\beta_1} x(t')dt', \tag{7}$$

indicating that the dynamics of the internal degree of freedom $x_1(t)$ is affected by the displacement $x(t)$ with a time lag of $\tau=\beta_1/k_1$. Several methods can be used to decouple the two variables in Eqs. (5) and (6). An integrodifferential equation for $x(t)$ can be obtained by substituting solution (7) into Eq. (6). The simplest approach is to apply the operator $(k_1/\beta_1)+d/dt$ to Eq. (6) and to use the identity $\beta_1\ddot{x}_1+k_1\dot{x}_1 = k_1\dot{x}$ (the derivative of Eq. (5)) to obtain a third-order linear differential equation for the oscillator coordinate $x(t)$,

$$m\dddot{x} + \tilde{\beta}\ddot{x} + (k_0 + \tilde{k}_1)\dot{x} + \frac{k_0 k_1}{\beta_1}x = 0, \tag{8}$$

where $\tilde{k}_1=k_1(1+\beta/\beta_1)$ and $\tilde{\beta}=\beta+mk_1/\beta_1$. Note that x_1 obeys a similar equation, which can be seen by solving Eq. (5) for x, taking the appropriate derivatives and then substituting the results into Eq. (6).

In the weak damping limit[17] the corresponding algebraic equation for a trial exponential solution $e^{\alpha t}$ of Eq. (8) yields two complex conjugate roots (associated with a damped oscillation) and a real negative root associated with a relaxation process. Thus, the general solution for $x(t)$ can be written in the form of a superposition of an exponentially damped oscillation on an exponentially decaying baseline,

$$x(t) = Ae^{-\gamma t}\sin(\omega t + \phi) + Be^{-\eta t}, \tag{9}$$

where ω, γ, and η depend on the model parameters and the constants A, B, and ϕ depend on the initial conditions defined by $x(0)$, $\dot{x}(0)$, and $\ddot{x}(0)$. In contrast to the viscously damped oscillator, $\ddot{x}(0)$ is not unambiguously defined by $x(0)$ and $\dot{x}(0)$ because the state of the internal degree of freedom is unknown. The form of solution (9) differs qualitatively from the usual damped harmonic oscillator due to the second term associated with the real solution of the characteristic equation. For some initial conditions this exponential background can be made negligible (for instance, by choosing $x(t)=x_0=0$ for $t\leq 0$ and $\dot{x}(0)=v_0$ generated by an impulse on the cart) so that the motion is indistinguishable from that predicted for a damped harmonic oscillator, thus justifying the empirical fitting function used to model the experimental data.

The viscoelastic nature of the system is displayed by the dependence of ω and γ on the parameters m, k_0, k_1, and β. To determine this dependence we substitute Eq. (9) differentiated up to three times into Eq. (8) and then set the coefficients of $e^{-\gamma t}\sin(\omega t+\phi)$, $e^{-\gamma t}\cos(\omega t+\phi)$, and $e^{-\eta t}$ to zero, leading to the system of equations

$$m\gamma(3\omega^2 - \gamma^2) + \tilde{\beta}(\gamma^2 - \omega^2) - (k_0 + \tilde{k}_1)\gamma + \frac{k_1 k_0}{\beta_1} = 0, \tag{10}$$

$$m\omega(3\gamma^2 - \omega^2) - 2\gamma\omega\tilde{\beta} + (k_0 + \tilde{k}_1)\omega = 0, \tag{11}$$

$$-m\eta^3 + \tilde{\beta}\eta^2 - (k_0 + \tilde{k}_1)\eta + \frac{k_1 k_0}{\beta_1} = 0. \tag{12}$$

Equation (12) will not be used and is given for completeness.

We divide Eq. (11) by $m\omega$ and solve it for ω^2 to obtain the angular frequency of the oscillator as a function of the model parameters and γ,

$$\omega^2 = \frac{k_0 + k_1\left(1 + \frac{\beta}{\beta_1}\right)}{m} + 3\gamma^2 - 2\gamma\left(\frac{k_1}{\beta_1} + \frac{\beta}{m}\right). \tag{13}$$

To obtain an independent equation for γ, we add Eq. (10) to Eq. (11) multiplied by γ/ω and find

$$2m\gamma(\omega^2 + \gamma^2) = m\left(\frac{k_1}{\beta_1} + \frac{\beta}{m}\right)(\omega^2 + \gamma^2) - k_0\frac{k_1}{\beta_1}. \tag{14}$$

If we substitute Eq. (13) into Eq. (14), move all terms involving γ to the left-hand side, and solve for γ in the factorized $2m\gamma$ term, we obtain after some algebra

$$\gamma = \frac{\frac{k_1}{2}\left(\frac{k_1}{\beta_1} + \frac{\beta}{m}\right)\left(1 + \frac{\beta}{\beta_1}\right) + \frac{\beta k_0}{2m}}{k_0 + k_1\left(1 + \frac{\beta}{\beta_1}\right) + m\left[2\gamma - \left(\frac{k_1}{\beta_1} + \frac{\beta}{m}\right)\right]^2}, \tag{15}$$

which is a convenient iterative equation for γ with excellent convergence properties in the range of reasonable model parameters. The solution for γ and ω^2 as a function of m is obtained for fixed k_0, k_1, β_1, and β by iterating Eq. (15) until convergence is obtained. (Three iterations are usually sufficient, and the first iteration with $\gamma=0$ is usually within 5% of the converged result.) The result for γ is then inserted into Eq. (13) to obtain $\omega^2(m)$.

In the $k_1\to 0$ limit the results for the damped harmonic oscillator are recovered. In the $\beta\to 0$ limit the viscoelastic element reduces to a standard linear solid model, which retains the phenomenology associated with the internal degree of freedom with a slightly simpler algebra. In this case in the low mass limit, the damping factor of the viscoelastic oscillator approaches a finite limit

$$\lim_{m\to 0}\gamma = \frac{k_1^2}{2\beta_1(k_0 + k_1)}, \quad \omega^2 \simeq \frac{k_0 + k_1}{m}. \tag{16}$$

Thus, in the limit $m\to 0$ the damped harmonic oscillator goes to the overdamped regime, and the viscoelastic model with $\beta=0$ displays only weakly damped oscillations. For $m\to\infty$ we retain only the dominant term k_1/β_1 in the denominator of Eq. (15), and $\gamma(m)$ approaches the damped harmonic oscillator limit with viscous parameter β_1

$$\lim_{m\to\infty}\gamma(m) \simeq \frac{\beta_1}{2m}, \quad \omega^2 \simeq \frac{k_0}{m}. \tag{17}$$

In the $k_1\to\infty$ limit the viscoelastic model reduces to the damped harmonic oscillator with parameters k_0 and β_1 as can

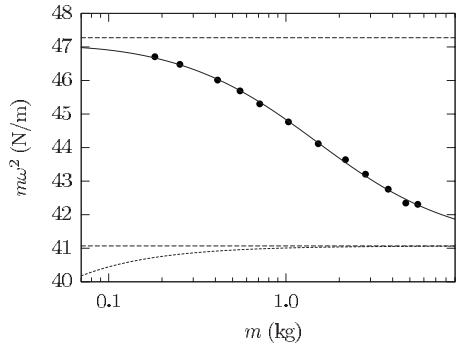

Fig. 5. Effective elastic response $m\omega^2$ of the rubber oscillator as a function of the mass m. The data (●) are compared with the model function (13) (solid curve). The low and high mass limits k_0+k_1 and k_0 are given as dashed lines. The prediction for the damped harmonic oscillator with the fitted k_0 and $\beta=0.5$ N s/m is a short dashed curve.

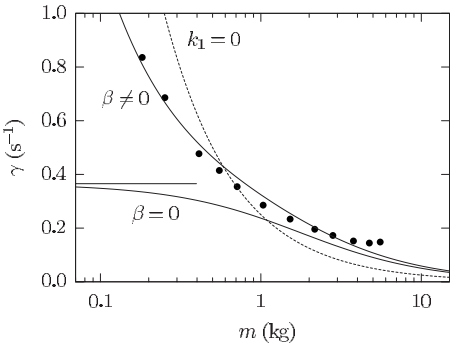

Fig. 6. The damping parameter γ as a function of the oscillator mass m. The data (●) are compared with the predictions of Eq. (3) for a damped harmonic oscillator with $\beta=0.5$ Ns/m ($k_1=0$, short dashed curve) and viscoelastic oscillators with three parameters ($\beta=0$) and four parameters ($\beta\neq 0$).

be seen by the corresponding limit of Eq. (8) multiplied by β_1/k_1.

IV. RESULTS

The behavior of the viscoelastic model is in qualitative agreement with the experimental data. The data analysis was performed by fitting Eqs. (13) and (15) to the experimental data. The resulting model parameters are $k_0=41.1\pm0.1$ N/m, $k_1=6.2\pm0.1$ N/m, $\beta_1=1.12\pm0.01$ N s/m, and $\beta=0.17\pm0.1$ N s/m. The relaxation time constant for the Maxwell element is $\tau=\beta_1/k_1=0.181\pm0.005$ s. The results for the mass dependence of $m\omega^2$ are shown in Fig. 5. The data display a crossover from the low mass high frequency limit k_0+k_1 to the high mass low frequency behavior k_0 (horizontal dashed lines), which differ by 15% and are nicely interpolated by solid curve (13) predicted by the model. The results of damped harmonic oscillator model (4) are unable to model the experimental behavior for any parameter set. We emphasize that the key element for obtaining the correct functional dependence is the inclusion of the Maxwell viscoelastic element with the parameters k_1 and β_1. Equivalent fits of the $\omega(m)$ dependence are obtained with a three parameter viscoelastic model (with $\beta=0$) whose treatment involves somewhat simpler algebra and is more suitable to be introduced in elementary courses. This result also means that β cannot be fit reliably based on the $\omega(m)$ data alone. The crossover displayed by the data is instead sufficient to fit k_0 and k_1, which determine the two asymptotic baselines of $m\omega^2$ and β_1, which together with k_1 determine the crossover frequency.

If the viscoelastic model in Fig. 4 is subject to a constant force and sufficient time is allowed for equilibration, then the internal degree of freedom relaxes, and the relations between force and displacement allow for the determination of k_0. Thus k_0 can be determined using static measurements, which are possible using standard laboratory procedures such as hanging different masses to both rubber bands in parallel to match the result of the dynamical experiment and measuring displacements in the vertical directions. We found $k_{\text{static}}=39\pm3$ N/m, which is consistent with k_0. In this case the major uncertainty comes from the measurement of the displacement of the equilibrium position, which is determined to about 5% due to creep effects with 1–2 cm total displacement. These creep effects are associated with long relaxation times not included in our model.

The mass dependence of γ is shown in Fig. 6 and compared with Eq. (15). The agreement with the prediction of the four parameter viscoelastic model is satisfactory. The inadequacy of the damped harmonic oscillator prediction (equivalent to the one shown in Fig. 3) is emphasized by the short dashed curve. The $\gamma(m)$ plot calculated with the k_0, k_1, and β_1 parameters for the standard linear solid model (with $\beta=0$ and the $m\to 0$ limit) fitted on the $\omega(m)$ data is also shown not to be adequate. This discrepancy demonstrates the inadequacy of a simple three parameter viscoelastic model to fit the $\gamma(m)$ dependence of the rubber oscillator, indicating that damping is only partly associated with the degrees of freedom with relaxation times on a time scale of seconds. The improved agreement with the four parameter viscoelastic model indicates that part of the viscous damping $\beta/\beta_1\simeq 0.15$ is associated with degrees of freedom with much shorter relaxation times that appear fully relaxed in the probed frequency range.

We emphasize that due to the similarity between the solutions of the viscoelastic and the damped harmonic oscillators (apart from the exponentially decaying background that may be hidden by large amplitude oscillations or depressed by the initial conditions), the viscoelastic nature of the system is not obvious from the analysis of a single $x(t)$ curve, and it is better emphasized by the mass dependence of ω and γ. The matching of the experimentally determined $\omega(m)$ and $\gamma(m)$ with a reasonable set of viscoelastic model parameters k_0, k_1, β_1, and β is a strong indication that such a model provides an accurate description of the rubber band oscillator.

V. DISCUSSION AND CONCLUSIONS

The data demonstrate the complexity of the dynamical behavior of a mass-rubber band oscillator, which cannot be described by a simple damped harmonic oscillator model but requires inclusion of viscoelastic elements. A linear viscoelastic model with four parameters and a single internal relaxation time predicts the observed dependence of ω and γ on m and the crossover between high frequency (low mass) to low frequency (high mass or static) behavior.

The limitations of such a linear four parameter model are also clear. The apparent weak dependence of the frequency on the amplitude cannot be explained by a linear model. Typical examples of nonlinear oscillators treated in introductory courses are associated with conservative systems with a nonparabolic potential such as the pendulum. In the rubber band case the nonlinearity of the equilibrium force as a function of its extension arises mostly from the Gaussian nature of the end-to-end probability distribution of the polymers[11] and is described in the simplest approximation by the Guth equation of state.[11,18] Nonlinear effects of even order cancel due to the disposition of the rubber bands on the two sides of the mass, and the third-order term vanishes for small amplitude motion. The nonlinearity here originates from the properties of polymers involving damping and nonlinear memory effects. To take these effects into account would go beyond the possibility of any linear oscillator model and the scope of this article.

Although the ability of the model to describe the $\omega(m)$ data is excellent, slight deviations for the $\gamma(m)$ data (although within the experimental uncertainty) are found, which are an indication of the limitations of the model of the damping mechanism. It is expected that a model with a single relaxation time will become less adequate if the frequency range is extended. For our experimental conditions, however, the entire set of data associated with the range of masses applicable to our experimental apparatus is well described by the viscoelastic model with four parameters. Given these limitations, the model is quite successful, especially as a first step beyond the damped harmonic oscillator description.

The physical interpretation of the four parameter model is instructive. The parameter k_0 represents the elastic response of rubber when the internal degrees of freedom are in equilibrium. When the oscillation has a frequency comparable or higher than $1/\tau$, the internal degrees of freedom do not have time to equilibrate during the motion and contribute to the increased stiffness of the system by about 15%. The macroscopic relaxation time $\tau \simeq 0.18$ s displayed by rubber is associated with the long relaxation times of the polymer conformations that, in the presence of a quick change in the rubber extension, do not have time to relax to the statistically more favored shapes driving the system out of thermodynamic equilibrium. Still the system responds with a well defined and measurable restoring force, which is about 15% greater than the force at equilibrium.

The pedagogical value of such an experiment is that students can take accurate experimental data and are challenged to evaluate the ability of models to explain the observed behavior. By doing a simple analysis it is possible to realize the inadequacy of the damped harmonic oscillator model and demonstrate how the model can be improved to explain qualitative and quantitative aspects of the data.

APPENDIX: DATA ACQUISITION DETAILS

The optical sensor was made of a highly collimated red LED with a $\lesssim 10°$ light emission cone shining in the direction of an optoschmitt sensor (integrating a photodiode, a current amplifier, and a Schmitt trigger) both rigidly mounted on a U shaped support. The required dc power source (5 V) was taken from one of the computer USB ports. The red LED produces visible light, which is useful in the alignment and matches the infrared spectral sensitivity peak of the sensor reasonably well. The lenses integrated in the devices provide a minimal optical focalization and the resolution can be improved by placing a slit (two pieces of dark Scotch tape are sufficient for resolutions down to 100 μm) with a suitable orientation in front of the sensor.

When an opaque object travels through the light path, the sensor probes the changes in the light intensity generating logical transitions in the electrical signal. When an opaque object cuts the light, the logical TTL output signal performs a $1 \rightarrow 0$ transition (from light to dark). Similarly, when its shadow leaves the detector, it performs a $0 \rightarrow 1$ transition. This optical gate can be used in various timing applications involving periodic motion and can also be converted into an encoder useful to acquire high precision displacement-time data for mechanical systems with one degree of freedom. The simplest implementation of a linear encoder is realized by coupling the optical gate with a scale made of a transparent rigid support on which a sequence of identical parallel opaque segments of width D is traced at a distance $\Delta x = 2D$. The scale can be easily produced by printing the desired graphical pattern on a transparent support with a laser printer. Good results with tolerances in the 10 μm range are achievable in this way. To obtain complete darkening the slit aperture in front of the optical sensor should be smaller than the width D of the segments. The encoder scale is fixed to the moving mechanical system with the lines orthogonal to the traveling direction. During motion the encoder scale will pass through the optical gate fixed in the laboratory frame, and each dark segment will generate a sequence of $1 \rightarrow 0$ and $0 \rightarrow 1$ transitions.

To probe the sequence of logical transitions, we used the computer parallel port (normally used as a printer port), which satisfies the IEEE-1284 standard, and is available on many motherboards at no additional cost. The signal pin from the optoschmitt detector can be conveniently connected to pin 10 of the 25 pin sub-D connector of the computer corresponding to bit S6 of the STATUS register, which is also the input for the IEEE-1284 interrupts (IRQ7). Ground is connected to any of the pins 18–25.

To activate the interrupt detection capability, the parallel port driver has to be loaded with the command `insmod parport_pc io=0×378 irq=7` using the Linux operating system. The acquisition is made with software written in C exploiting the low level I/O functions defined by the `ppdev` driver.[19] The changes of the S6 bit can be monitored by successive readouts of the STATUS register using low level `ioctl` functions such as `ioctl(fd,PPRSTATUS,&ch);` where `unsigned char ch;` is a byte variable and `fd` is the file descriptor associated with the parallel port as defined by the corresponding `open` statement. Alternatively the $0 \rightarrow 1$ transitions on S6 can also be revealed as interrupt signals using the system function `select`. For this purpose `fd` has to be included in the set of file descriptors being monitored using the C functions `FD_ZERO` and `FD_SET`. The timing of logical transition events is made using the system clock,[20] which can be rapidly accessed (<1 μs) via software using the C function `gettimeofday`. The system clock pace can be finely tuned with the `adjtimex` command if required.

A basic data acquisition algorithm consists of a sequence of an interrupt-waiting routine, probing for the $0 \rightarrow 1$ transitions on the parallel port input, followed by a time reading function. An example of a minimal C code fragment follows:

```
#include <linux/fd.h>
#include <linux/ppdev.h>
#include <fcntl.h>
#include <sys/time.h>
#include <unistd.h>
  int fd, irqc, retval; double t0, t1, x, dx;
  fd_set rfds;
  struct timeval tt1; struct timezone ttz;
main() {
  fd=open ("/dev/parport0", O_RDWR);
  ioctl(fd, PPCLAIM);
  FD_ZERO (&rfds); FD_SET (fd, &rfds);
  t0=0; x=0; dx=0.0010375;
  for(;;) {
  ioctl(fd,PPCLRIRQ, &irqc);
  retval=select(fd+1,&rfds,NULL,NULL,NULL);
  gettimeofday(&tt1,&ttz);
  t1=(double)(tt1.tv_sec)+
(double)(tt1.tv_usec)/1000000;
  if(!t0)t0=t1;
  printf("%lf %lf\n", x, t1-t0);
  x+=dx;
}}
```

In this simple implementation the computer will reveal every $0\rightarrow 1$ transition as an interrupt signal so that the timing process will generate a train of time values corresponding to the successive dark-transparent edges of the encoder scale. The first interrupt signal will be assigned to the origin of the space and time coordinates ($x=0$, $t=0$), and (for motion that does not involve speed reversal) the n interrupt will correspond to position $n\Delta x$. By associating each time with the corresponding coordinate, a position-time curve is obtained. In this way the linear motion of the body is sampled at equal space intervals $\Delta x=1.0375$ mm in our case. With some additional alignment effort, it is possible to work with $\Delta x \simeq 0.5$ mm to increase sampling. The precision of the encoder is limited only by the timing performance of the computer (μs range) and by the accuracy of the scale tracing (μm range).

For motion involving inversions of the sign of the velocity, the algorithm has to be improved. We kept the hardware (and alignment) as simple as possible and implemented an algorithm for this purpose. When the velocity v changes sign, $|v|$ passes through a minimum that results in a maximum in the sequence of time intervals between successive interrupts and can be easily identified. The motion inversion may occur in the shaded (case 1) or illuminated (case 2) regions, as illustrated in Fig. 7. The analysis of the problem for hardware that detects only dark-light transitions and for a regular displacement-time curve with a parabolic maximum indicates that the largest time interval almost always contains the inversion apart from a few special cases indicated by $-a$. When the maximum displacement is just above an edge between dark and transparent regions, the inversion occurs in the interval successive to the longest one (case $2-a$); when it occurs just above an edge between transparent and dark regions, the inversion occurs in the interval previous to the longest one (case $1-a$). To unambiguously identify which case is involved, it is necessary to check a sequence of four time intervals: $\Delta t_i=t_i-t_{i-1}$, $i=1,2,3,4$. All inversions are characterized by the conditions

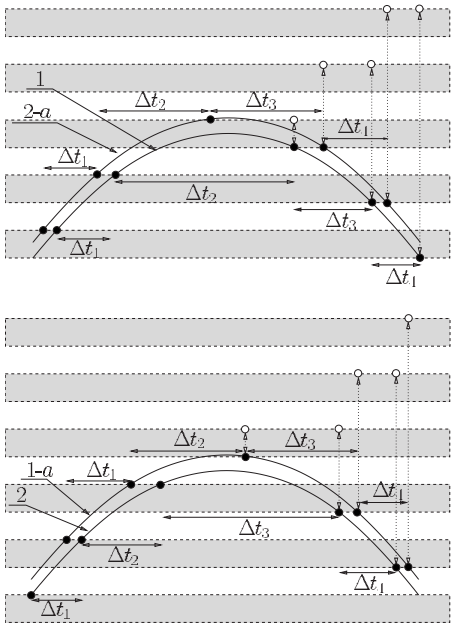

Fig. 7. Schematic of the inversion detection algorithm for a parabolic maximum placed on the sequence of dark encoder segments (shaded regions). The ● symbol refers to the actual displacement-time values, and the ○ symbol refers to the assumed displacement-time values in the absence of the correction for the velocity inversion. The vertical dashed lines indicate the required corrections. Cases 1 and $2-a$ (upper panel) and 2 and $1-a$ (lower panel) are illustrated.

$$\Delta t_1 < \Delta t_2 \cap \Delta t_1 < \Delta t_3 \cap \Delta t_4 < \Delta t_3 \cap \Delta t_4 < \Delta t_2. \quad \text{(A1)}$$

The required displacement corrections are the same for the cases 2 and $2-a$, and for cases 1 and $1-a$, they can be distinguished by a further condition on Δt_1 and Δt_4,

$$1 \text{ and } 1-a, \quad \Delta t_1 > \Delta t_4, \quad x_2 \rightarrow x_2 - \tfrac{1}{2}\Delta x, \quad \text{(A2)}$$

$$2 \text{ and } 2-a, \quad \Delta t_1 < \Delta t_4, \quad x_3 \rightarrow x_3 - \tfrac{3}{2}\Delta x. \quad \text{(A3)}$$

After the correction it is sufficient to change the sign of the Δx ($\Delta x \rightarrow -\Delta x$) to invert the direction of motion in the software and resume the normal incremental procedure. The condition that the average speed in the interval is smaller than a suitable threshold is required to avoid the condition (A1) being satisfied due to noise.

An intrinsic limitation of the present low-cost solution is in the sequential (not real time) execution of the instructions of the compiled code by the CPU. The computer may pause the execution between a transition detection and the subsequent time readout, introducing an unknown uncertainty in the timing. Our experience has shown that if the CPU is not loaded by other tasks, the occurrence of latency events is negligible, and apart from sporadic cases that are easily identified, this acquisition approach is capable of 10 μs timing accuracy and 10 μm space accuracy at a negligible cost. With this approach the students can be involved in hardware optimization and in writing elementary acquisition software.

[1] L. P. Fulcher and B. F. Davis, "Theoretical and experimental study of the motion of the simple pendulum," Am. J. Phys. **44**, 51–55 (1976).
[2] S. D. Schery, "Design of an inexpensive pendulum for study of large-angle motion," Am. J. Phys. **44**, 666–670 (1976).
[3] T. Lewowski and K. Woźniak, "The period of a pendulum at large am-

plitudes: A laboratory experiment," Eur. J. Phys. **23**, 461–464 (2002).
[4] F. M. S. Lima and P. Arun, "An accurate formula for the period of a simple pendulum oscillating beyond the small angle regime," Am. J. Phys. **74**, 892–895 (2006).
[5] I. R. Lapidus, "Motion of a harmonic oscillator with sliding friction," Am. J. Phys. **38**, 1360–1361 (1970).
[6] R. C. Hudson and C. R. Finfgeld, "Laplace transform solution for the oscillator damped by dry friction," Am. J. Phys. **39**, 568–570 (1971).
[7] A. Marchewka, D. S. Abbott, and R. J. Beichner, "Oscillator damped by a constant-magnitude friction force," Am. J. Phys. **72**, 477–483 (2004).
[8] A. Ricchiuto and A. Tozzi, "Motion of a harmonic oscillator with sliding and viscous friction," Am. J. Phys. **50**, 176–179 (1982).
[9] P. T. Squire, "Pendulum damping," Am. J. Phys. **54**, 984–991 (1986).
[10] A. Yariv, J. Scheuer, B. Crosignani, and P. Di Porto, "The case of the oscillating party balloon: A simple toy experiment requiring a not-so-simple interpretation," Am. J. Phys. **75**, 696–700 (2007).
[11] L. R. G. Treloar, "The elasticity and related properties of rubbers," Rep. Prog. Phys. **36**, 755–826 (1973).
[12] L. R. G. Treloar, *The Physics of Rubber Elasticity*, 3rd ed. (Clarendon, Oxford, 1975).
[13] F. J. Lockett, *Nonlinear Viscoelastic Solids* (Academic, New York, 1972).
[14] J. Ferry, *Viscoelastic Properties of Polymers* (Wiley, New York, 1980).
[15] R. M. Christensen, *Theory of Viscoelasticity* (Academic, New York, 1982).
[16] Y. Ketema, "Approximate model for a viscoelastic oscillator," J. Appl. Mech. **70**, 757–761 (2003).
[17] P. Muller, "Are the eigensolutions of a 1-d.o.f. system with viscoelastic damping oscillatory or not?," J. Sound Vib. **285**, 501–509 (2005).
[18] H. M. James and E. Guth, "Statistical thermodynamics of rubber elasticity," J. Chem. Phys. **21**, 1039–1049 (1953).
[19] T. Waugh, "The Linux 2.4 parallel port subsystem," ⟨kernelbook.sourceforge.net/parportbook.pdf⟩.
[20] A. Rubini and J. Corbet, *Linux Device Drivers*, 2nd ed. (O'Reilly & Associates, Sebastopol, 2001).